Partial Differential Equations in Applied Mathematics 13 (2025) 101084

Contents lists available at ScienceDirect

Partial Differential Equations in Applied Mathematics

journal homepage: www.elsevier.com/locate/padiff

Comparative rheological features of radiated Darcy-Forchheimer flow of micropolar and second grade fluid with cross diffusion and Arrhenius activation energy

S. Bilal [a], Muhammad Yasir [b,*], Ali Hasan Ali [c,d]

[a] Department of Mechanical Engineering, College of Engineering, Prince Mohammad Bin Fahd University, Al Khobar 31952, Saudi Arabia
[b] Department of Mathematics, Quaid-i-Azam University, Islamabad 44000, Pakistan
[c] Department of Business Management, Al-imam University College, 34011 Balad, Iraq
[d] Technical Engineering College, Al-Ayen University, Dhi Qar 64001, Iraq

ARTICLE INFO

Keywords:
Riga plate
Second grade fluid
Micropolar fluid
Buongiorno model
Stretching surface

ABSTRACT

The main intension of this study is to scrutinize the transient flow characteristics of two different non-Newtonian models of micropolar fluid and second grade fluid subject to a stretchable Riga plate. This novel study communicates with the rotational motion of microelements by taking into account the strong and weak concentrations and incompressible Darcy Forchheimer flow features of second grade fluid. In the context of Dufour and Soret effects, the cross-diffusion process is analyzed in the mechanisms of mass and heat transport. Moreover, Buongiorno model is taken into account to deliberate the random movement of particles and thermophoretic effects in both considered fluids. The consequences of convective constraint, Arrhenius activation energy, and joule heating are also incorporated. The framework of ordinary dimensionless equations is accomplished by deploying convenient variables and numerically processed via reliable bpv4c technique in MATLAB. The rheology of both considered fluids is compared through graphics regarding different concentration level and pertinent parameters. Micropolar fluid has higher intensity of its dynamical behavior as compared to second grade fluid. Moreover, the improved activation energy parameter lowers the nature of both considered fluids.

1. Introduction

Over the years, the theory of micropolar fluids has garnered significant interest among scientists due to the inability of traditional Newtonian fluid models to accurately describe the behavior of fluids containing rigid particles. This theory considers fluids as suspensions of small, rigid particles, such as dumbbell-shaped molecules, which exhibit rotational motion in addition to translational movement. The rotational dynamics of these molecules are a defining feature of micropolar fluids, which find applications in various fields, including colloidal suspensions, liquid crystals, blood rheology, the behavior of animal blood, the influence of dirt on general fluid behavior, and lubrication on porous surfaces. Eringen [1,2] first discussed the theory of micropolar fluid to spectacle the effects of combined stress and native rotatory inertia. Through a vertical medium, the transient based flow mechanism influenced by distinct physical constraints in a micropolar fluid was portrayed by Chamkha et al. [3]. An exploration of micropolar fluid in a channel through HPM was estimated by Sheikholeslami et al. [4]. An outstanding appraisal of micropolar fluids and their tenders were obtainable by Pal and Chatterjee [5]. The dynamics of the flow past a stretchable plate with nonlinear properties in a micropolar fluid was inspected by Zaimi and Ishak [6]. Through an absorbable medium, Abdollahzadeh Jamalabadi [7] discussed the concentrated flow phenomenon through analytical technique in a micropolar fluid. Noreen et al. [8] examined electroosmosis-driven thermal transfer in Jeffrey fluid flow via the curved porous channel. On the dynamics of micropolar fluid, more studies are elucidated in Refs. [9–14].

The second-grade fluid, a type of differential non-Newtonian fluid model, is utilized in the current study. Second-grade fluids with their viscoelastic nature proposed interesting implementations including lubrication technology, geophysical flows, petroleum industry, and painting processes. Jamil et al. [15] investigated the helical flows within two coaxial containers for second grade fluid. The twofold and thrice solutions of magnetized 2nd grade fluid in the existence of slip conditions were presented by Turkyilmazoglu [16]. The unsteady motion of

* Corresponding author.
E-mail address: myasir@math.qau.edu.pk (M. Yasir).

https://doi.org/10.1016/j.padiff.2025.101084
Received 20 September 2024; Received in revised form 2 December 2024; Accepted 8 January 2025
Available online 10 January 2025

Nomenclature

Sc	Schmidt number
$\widetilde{\sigma}$	Electrical conductivity
Du	Dufour parameter
$(\widetilde{V},\widetilde{U})$	Velocity components
κ_r	Reaction rate
$\widetilde{\rho}$	Density
α^*	Second grade fluid parameter
$\widetilde{C}_s$	Concentration susceptibility
Pr	Prandtl number
$\widetilde{\vartheta}$	Kinematic viscosity
$\widetilde{j}$	Microinertia coefficient
$\widetilde{h}$	Convective heat transfer coefficient
$\widetilde{D}_{\widetilde{B}}$	Brownian motion coefficient
γ	Biot number
k_1	Thermal conductivity
S	Unsteadiness parameter
$\widetilde{C}_{\widetilde{p}}$	Specific heat capacity
Nb	Brownian motion parameter
κ_o	Chemical reaction parameter
$(\widetilde{Y},\ \widetilde{X})$	Cartesian coordinates
$\widetilde{\alpha}$	Thermal diffusivity
δ_1	Second grade fluid parameter
$\kappa_{\widetilde{T}}$	Thermal diffusion
$\widetilde{M_o}$	Magnetization of magnets
θ_w	Temperature difference parameter
ε^*	Porosity parameter
$\widetilde{D}_{\widetilde{T}}$	Thermophoresis coefficient
β_0	Magnetic field strength
m_o	Surface boundary parameter
M^*	Magnetic parameter
k^*	Boltzmann constant
Sr	Soret parameter
F_r	Dracy Forchheimer parameter
Nt	Thermophoresis parameter
E^*	Activation energy
K	Micropolar fluid parameter
$\widetilde{j_o}$	Current density
E	Activation energy parameter
$\widetilde{k}$	Vortex viscosity
Ec	Eckert number

wall persuaded according to time dependent flow of fluid was examined by Zheng et al. [17]. Srinivasa et al. [18] studied the thermal effects in Stokes' second problem resulted in magnetic field for second grade fluid through permeable surface. The viscoelastic fluid-soaked absorbent module with rotatory motion in need of mechanical vibration was explored by Bhadauria and Kiran [19]. The boundary layer flow corresponding to both rigorous and applicable method in a viscoelastic fluid characterized by Newtonian heating was inspected by Rahman et al. [20]. On a cylindrical stretched medium, consequences of cross diffusion on the thermal characteristics of a second-grade fluid were portrayed by Shojaei et al. [21]. Vaidya et al. [22] studied the peristaltic process of magnetized non-Newtonian nanofluids in order to maximize fluid flow and heat transfer. Bhandari et al. [23] characterized Newtonian fluid flow features and heat transfer in vertical microchannels that are susceptible to cyclic membrane contraction because of buoyancy forces and pressure gradients. More explorations on second grade fluid are depicted in Refs. [24–28].

In recent times, nanofluid theory is studied numerically and experimentally by some researchers and observed to have comprehensive applications in distinct disciplines including electronic devices, fuel cell, chiller, nuclear reactor, and hybrid powered engines etc. Nanofluid achieve the goals in cancer treatment, optical grating, and to escort the spots up in the bloodstream to a tumor with magnets. The submerging of nanoparticles in base fluid enhances the thermal performance of ordinary heat transfer fluids and thermal conductivity. The concept of nanofluid was initially developed by Choi [29]. The scattering of ultra-fine particles in the base fluid with the variation in the viscosities of fluid and thermal conductivities was investigated by Noghrehabadi et al. [30]. The nanofluid flow and heat transfer in a porous channel by using KKL relationships for simulation was addressed by Kandelousi [31]. Turkyilmazoglu [32] presented single and multi-phase models for the condensation of heat transfer and nanofluid film flow. He indicated that more intensifies heat transfer is detected as diffusion parameter increases in the multi-phase model. The features of motivation energy in magnetized nanofluids flow verses absorbant medium was reported by Bhatti et al. [33]. Nasir et al. [34] used the Darcy-Forchheimer model to investigate how entropy generation and radiation role affected the dynamics of nanofluid in porous medium. The more related studies are elucidated in Refs. [35–42].

In view of the aforementioned studies, micropolar fluids have been extensively studied but the flow mechanism of micropolar fluid along with second grade fluid relative to a Riga stretchable plate with Buongiorno model and Arrhenius activation energy is not scrutinized until now. The current novel study covers the transient flow behavior of both micropolar fluid and second grad fluid with their incompressible characteristics. A Riga plate with stretchable motion is taken to deliberate the transient flow attributes of both considered fluids in two dimensions. The rotational movement of microelements in micropolar fluid are taken on both weak and strong concentrations. The Brownian movement of molecules and thermophoretic consequences are encountered via Buongiorno model. The influences of cross diffusions, joule heating, and Arrhenius activation energy with convective constraint are encompassed in mass and heat phenomenon. The dynamics of both considered fluids are comparatively analyzed through graphical approach.

2. Problem formulation

To develop the mathematical model, two distinct micropolar and second grade fluids are analyzed with their transient characteristics over a Riga stretchable surface. The incompressible Darcy Forchheimer based flow behavior of fluid in two dimensions is explored in the system of Cartesian coordinates. The $\widetilde{X}$-axis is positioned along with considered Riga sheet which is stretched with velocity $\widetilde{U}_w$. On the other hand, the $\widetilde{Y}$-axis takes the position above the $\widetilde{X}$-axis in perpendicular direction (See Fig. 1). Micropolar fluid is considered to have both string and weak concentrations. Both fluids are thermally scrutinized through joule heating, Buongiorno model, thermal diffusion, and convective constraint. The transport mechanism of mass in micropolar fluid and second grade fluid is conducted via mass diffusion and Arrhenius activation energy.

Based on physical assumptions and simplifications, the equations concerning the flow problem are manifested as follows [12,26,43,44]:

$$\frac{\partial \widetilde{V}}{\partial \widetilde{Y}} = -\frac{\partial \widetilde{U}}{\partial \widetilde{X}}, \tag{1}$$

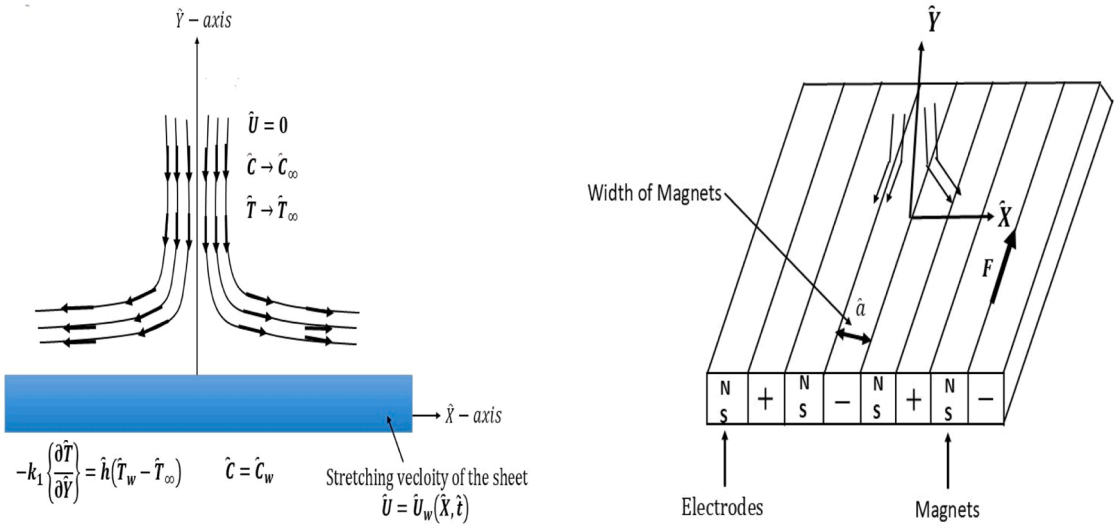

Fig. 1. Problem's schematic.

$$\widetilde{\vartheta}\left\{\frac{\partial^2\widetilde{U}}{\partial\widetilde{Y}^2}\right\}\left\{1+\frac{\widetilde{k}}{\widetilde{\mu}}\right\}-\left\{\frac{\partial\widetilde{U}}{\partial\widetilde{Y}}\right\}\widetilde{V}+\frac{\delta_1}{\widetilde{\rho}}\left(\left\{\frac{\partial^2\widetilde{U}}{\partial\widetilde{Y}^2}\right\}\left\{\frac{\partial\widetilde{U}}{\partial\widetilde{X}}\right\}+\left\{\frac{\partial^3\widetilde{U}}{\partial\widetilde{t}\partial\widetilde{Y}^2}\right\}+\left\{\frac{\partial^2\widetilde{V}}{\partial\widetilde{Y}^2}\right\}\left\{\frac{\partial\widetilde{U}}{\partial\widetilde{Y}}\right\}+\left\{\frac{\partial^3\widetilde{U}}{\partial\widetilde{Y}^3}\right\}\widetilde{V}+\left\{\frac{\partial^3\widetilde{U}}{\partial\widetilde{X}\partial\widetilde{Y}^2}\right\}\widetilde{U}\right)-\left\{\frac{\partial\widetilde{U}}{\partial\widetilde{t}}\right\}+\left\{\frac{\widetilde{M}_o\widetilde{\pi}\widetilde{j}_o}{8\widetilde{\rho}}\right\}e^{-\left(\frac{\widetilde{\pi}}{\widetilde{a}}\right)\widetilde{Y}}-\{\widetilde{U}^2\}\widetilde{F}\left\{\frac{1}{(\dot{k})^{1/2}}\right\}+\frac{\widetilde{k}}{\widetilde{\rho}}\left\{\frac{\partial N^*}{\partial\widetilde{Y}}\right\}-\widetilde{U}\left\{\frac{\partial\widetilde{U}}{\partial\widetilde{X}}\right\}-\widetilde{\vartheta}\left\{\frac{1}{\widetilde{k}}\right\}\{\widetilde{U}\}=0, \tag{2}$$

$$\left\{\frac{1}{\widetilde{\rho j}}\right\}\widetilde{\gamma}\left\{\frac{\partial^2N^*}{\partial\widetilde{Y}^2}\right\}-\left\{\frac{\partial N^*}{\partial\widetilde{X}}\right\}\widetilde{U}-\left\{\frac{1}{\widetilde{\rho j}}\right\}\widetilde{k}2N^*-\left\{\frac{\partial N^*}{\partial\widetilde{Y}}\right\}\widetilde{V}-\left\{\frac{1}{\widetilde{\rho j}}\right\}\widetilde{k}\left\{\frac{\partial\widetilde{U}}{\partial\widetilde{Y}}\right\}-\left\{\frac{\partial N^*}{\partial\widetilde{t}}\right\}=0, \tag{3}$$

$$-\left\{\frac{\partial\widetilde{T}}{\partial\widetilde{t}}\right\}+\widetilde{\alpha}\left\{\frac{\partial^2\widetilde{T}}{\partial\widetilde{Y}^2}\right\}+\widetilde{\tau}\left(\widetilde{D}_{\widetilde{B}}\left\{\frac{\partial\widetilde{T}}{\partial\widetilde{Y}}\right\}\left\{\frac{\partial\widetilde{C}}{\partial\widetilde{Y}}\right\}+\widetilde{D}_{\widetilde{T}}\left\{\frac{1}{\widetilde{T}_\infty}\right\}\left\{\frac{\partial\widetilde{T}}{\partial\widetilde{Y}}\right\}^2\right)-\left\{\frac{\partial\widetilde{T}}{\partial\widetilde{Y}}\right\}\widetilde{V}+D^*\kappa_{\widetilde{T}}\left\{\frac{1}{\widetilde{C}_s\widetilde{C}_{\widetilde{p}}}\right\}\left\{\frac{\partial^2\widetilde{T}}{\partial\widetilde{Y}^2}\right\}-\left\{\frac{\partial\widetilde{T}}{\partial\widetilde{X}}\right\}\widetilde{U}+\beta_0^2\widetilde{\sigma}\left\{\frac{1}{\widetilde{\rho}\widetilde{C}_{\widetilde{p}}}\right\}\widetilde{U}^2=0, \tag{4}$$

$$\widetilde{D}_{\widetilde{B}}\left\{\frac{\partial^2\widetilde{C}}{\partial\widetilde{Y}^2}\right\}-\left\{\frac{\partial\widetilde{C}}{\partial\widetilde{X}}\right\}\widetilde{U}+\widetilde{D}_{\widetilde{T}}\left\{\frac{1}{\widetilde{T}_\infty}\right\}\left\{\frac{\partial^2\widetilde{T}}{\partial\widetilde{Y}^2}\right\}+\left\{\frac{\partial\widetilde{C}}{\partial\widetilde{Y}}\right\}\widetilde{V}-(\widetilde{C}-\widetilde{C}_\infty)\kappa_r^2\left(\frac{\widetilde{T}_\infty}{\widetilde{T}}\right)^{\widetilde{n}}e^{\left(-\frac{k^*\widetilde{T}}{E^*}\right)^{-1}}-\left\{\frac{\partial\widetilde{C}}{\partial\widetilde{t}}\right\}+D^*\kappa_{\widetilde{T}}\left\{\frac{1}{\widetilde{T}_\infty}\right\}\left\{\frac{\partial^2\widetilde{T}}{\partial\widetilde{Y}^2}\right\}=0, \tag{5}$$

The appropriate conditions at the boundary are manifested as follows [11]:

$$\begin{aligned}
&\widetilde{V}=0,\\
&N^*=-m_o\left\{\frac{\partial\widetilde{U}}{\partial\widetilde{Y}}\right\},\\
&-k_1\left\{\frac{\partial\widetilde{T}}{\partial\widetilde{Y}}\right\}=\widetilde{h}(\widetilde{T}_w-\widetilde{T}_\infty),\\
&\widetilde{U}=\widetilde{U}_w,\\
&\widetilde{C}=\widetilde{C}_w \quad \text{at} \quad \widetilde{Y}=0,\\
&N^*\to0,\\
&\widetilde{T}\to\widetilde{T}_\infty,\\
&\widetilde{U}=0,\\
&\widetilde{C}\to\widetilde{C}_\infty \quad \text{as} \quad \widetilde{Y}\to\infty.
\end{aligned} \tag{6}$$

In the present mechanism, we adopt that $\widetilde{j}=\frac{\widetilde{\vartheta}}{\widetilde{a}}$, $\widetilde{\gamma}=\left\{\widetilde{\mu}+\frac{\widetilde{k}}{2}\right\}\widetilde{j}$.

The setup of adequate similarity variables is deliberated as follows [11]:

$$\begin{aligned}
&\zeta=\left\{\frac{1}{(\widetilde{Y})^{-1}}\right\}\left\{\frac{\widetilde{\vartheta}\widetilde{X}}{\widetilde{U}_w}\right\}^{-0.5},\\
&N^*=\widetilde{U}_wG(\zeta)\left\{\frac{\widetilde{\vartheta}\widetilde{X}}{\widetilde{U}_w}\right\}^{-0.5},\\
&\widetilde{C}=\widetilde{C}_\infty+\Phi(\zeta)[\widetilde{C}_w-\widetilde{C}_\infty],\\
&\psi=F(\zeta)\left\{\frac{1}{(\widetilde{\vartheta}\widetilde{X}\widetilde{U}_w)^{-0.5}}\right\},\\
&\widetilde{U}_w=\widetilde{a}\widetilde{X}\left\{\frac{1}{1-\widetilde{c}\widetilde{t}}\right\},\\
&\widetilde{T}=\ \theta(\zeta)[\widetilde{T}_w-\widetilde{T}_\infty]+\widetilde{T}_\infty.
\end{aligned} \tag{7}$$

After using the above transformations in Eqs. (1)-(5), we acquire

$$\left\{\frac{d^3F}{d\zeta^3}\right\}\{1+K\}+\alpha^*\left[-\left\{\left(\frac{d^2F}{d\zeta^2}\right)^2\right\}+2\left\{\frac{d^3F}{d\zeta^3}\right\}\{F(\zeta)\}-\left\{\frac{d^4F}{d\zeta^4}\right\}\{F(\zeta)\}+S\left(\left\{\frac{\zeta}{2}\right\}\left\{\frac{d^4F}{d\zeta^4}\right\}+2\left\{\frac{d^3F}{d\zeta^3}\right\}\right)\right]-\left\{\left(\frac{dF}{d\zeta}\right)^2\right\}+Me^{\lambda\zeta}-F_r\left\{\left(\frac{dF}{d\zeta}\right)^2\right\}+\left\{\frac{dG}{d\zeta}\right\}K+S\left(\left\{\frac{1}{2}\right\}\left\{\frac{d^2F}{d\zeta^2}\right\}\zeta+\left\{\frac{dF}{d\zeta}\right\}\right)+\left\{\frac{d^2F}{d\zeta^2}\right\}\{F(\zeta)\}-\epsilon^*\left\{\frac{dF}{d\zeta}\right\}=0, \tag{8}$$

$$\left\{\frac{d^2G}{d\zeta^2}\right\}\left(\left\{\frac{K}{2}\right\}+1\right)-S\left(\left\{\frac{1}{2}\right\}\left\{\frac{dG}{d\zeta}\right\}\zeta+\left\{\frac{3}{2}\right\}\{G(\zeta)\}\right)+\{F(\zeta)\}\left\{\frac{dG}{d\zeta}\right\}-\left\{\frac{d^2F}{d\zeta^2}\right\}K-\left\{\frac{dF}{d\zeta}\right\}\{G(\zeta)\}-2K\{G(\zeta)\}=0, \tag{9}$$

$$\left\{\frac{d^2\theta}{d\zeta^2}\right\}+Ec\left\{\frac{dF}{d\zeta}\right\}M^*\left\{\frac{dF}{d\zeta}\right\}Pr+\{F(\zeta)\}Pr\left\{\frac{d\theta}{d\zeta}\right\}+Du\left\{\frac{d^2\Phi}{d\zeta^2}\right\}Pr-\left\{\frac{dF}{d\zeta}\right\}Pr\{\theta(\zeta)\}+Nb\left\{\frac{d\Phi}{d\zeta}\right\}Pr\left\{\frac{d\theta}{d\zeta}\right\}-S\{\theta(\zeta)\}Pr+Nt\left\{\frac{d\theta}{d\zeta}\right\}\left\{\frac{d\theta}{d\zeta}\right\}Pr-S\left\{\frac{1}{2}\right\}Pr\left\{\frac{d\theta}{d\zeta}\right\}\zeta=0, \tag{10}$$

$$\left\{\frac{d^2\Phi}{d\zeta^2}\right\}+Sr\left\{\frac{d^2\theta}{d\zeta^2}\right\}Sc-\left\{\frac{1}{2}\right\}Sc\zeta\left\{\frac{d\Phi}{d\zeta}\right\}S-\kappa_o[\{\theta(\zeta)\}\theta_w+1]^{\tilde{n}}Sce^{\left(\frac{E}{\{\theta(\zeta)\}\theta_w+1}\right)}+\{F(\zeta)\}Sc\left\{\frac{d\Phi}{d\zeta}\right\}+\left\{\frac{1}{Nb}\right\}\left\{\frac{d^2\theta}{d\zeta^2}\right\}Nt=0. \tag{11}$$

Eqs. (6) and (7) yields the following outcomes

$$\begin{aligned}
&\left\{\frac{dF}{d\zeta}\right\}=1,\\
&\left\{\frac{d\theta}{d\zeta}\right\}=-\gamma\{1-\{\theta(\zeta)\}\},\\
&\{F(\zeta)\}=0,\\
&\{\Phi(\zeta)\}=1,\\
&\{G(\zeta)\}=-m_o\left\{\frac{d^2F}{d\zeta^2}\right\},\quad \text{at}\quad \zeta=0,\\
&\{\Phi(\zeta)\}=0,\\
&\left\{\frac{dF}{d\zeta}\right\}=0,\\
&\{G(\zeta)\}=0,\\
&\{\theta(\zeta)\}=0,\\
&\left\{\frac{d^2F}{d\zeta^2}\right\}=0,\quad \text{as}\quad \zeta\to\infty.
\end{aligned} \tag{12}$$

The parameters with dimensionless form involved in the above equations are expressed as follows

$$\begin{aligned}
\gamma&=\left\{\frac{\widetilde{\vartheta}(1-\widetilde{tc})}{\widetilde{a}}\right\}^{0.5}\left\{\frac{k_1}{\widetilde{h}}\right\}^{-1},\quad Nt=\{\widetilde{T}_w-\widetilde{T}_\infty\}\widetilde{D}_{\tilde{T}}\left\{\frac{1}{\widetilde{T}_\infty\widetilde{\vartheta}}\right\}\widetilde{\tau},\quad S=\left\{\frac{1}{\widetilde{\alpha}}\right\}\widetilde{c},\quad M\\
&=\widetilde{\pi}\left\{\frac{\widetilde{j_o}}{8\widetilde{\rho}\widetilde{U}_w^{\,2}}\right\}\widetilde{X}\widetilde{M}_o,\ Du=\left\{\frac{\kappa_{\tilde{T}}D^*}{\widetilde{T}_w-\widetilde{T}_\infty}\right\}\{\widetilde{C}_w-\widetilde{C}_\infty\}\left\{\frac{1}{\widetilde{\vartheta}}\right\}\left\{\frac{1}{\widetilde{C}_s\widetilde{C}_{\tilde{p}}}\right\},\quad Nb\\
&=\widetilde{D}_{\tilde{B}}\left\{\frac{1}{\widetilde{\vartheta}}\right\}\widetilde{\tau}\{\widetilde{C}_w-\widetilde{C}_\infty\},\quad \alpha^*=\delta_1\left\{\frac{1}{\widetilde{\mu}}\right\}\left\{\frac{1}{1-\widetilde{tc}}\right\}\widetilde{a},M^*=\beta_0^2\left\{\frac{1}{\widetilde{\rho}\widetilde{a}}\right\}\widetilde{\sigma},\quad Ec\\
&=\left\{\frac{1}{\widetilde{C}_{\tilde{p}}}\right\}\widetilde{U}_w^{\,2}\left\{\frac{1}{\widetilde{T}_w-\widetilde{T}_\infty}\right\},\quad Sc=\left\{\frac{1}{\widetilde{D}_{\tilde{B}}}\right\}\widetilde{\vartheta},\quad Sr\\
&=\{\widetilde{T}_w-\widetilde{T}_\infty\}\left\{\frac{1}{\widetilde{\vartheta}\widetilde{T}_\infty}\right\}\left\{\frac{\kappa_{\tilde{T}}D^*}{\widetilde{C}_w-\widetilde{C}_\infty}\right\},Pr=\left\{\frac{1}{\widetilde{\alpha}}\right\}\widetilde{\vartheta},\quad E=\left\{\frac{1}{\widetilde{T}_\infty k^*}\right\}E^*,\quad K\\
&=\left\{\frac{1}{\widetilde{\mu}}\right\}\widetilde{k},\quad \theta_w=\left\{\frac{1}{\widetilde{T}_\infty}\right\}\{\widetilde{T}_w-\widetilde{T}_\infty\},\ \epsilon^*=\{\widetilde{\vartheta}\}\left\{\frac{1}{\widetilde{k}\widetilde{c}}\right\},\quad \kappa_o=\left\{\frac{1}{\widetilde{a}}\right\}\kappa_r^2,\quad F_r\\
&=\widetilde{F}\left\{\frac{1}{(\dot{k})^{1/2}}\right\},
\end{aligned} \tag{13}$$

The quantities of physical interest are Sherwood number, skin friction coefficient, and Nusselt number which are manifested through the following relations [11,20,26]:

$$\begin{aligned}
\overline{Sh}_{\tilde{X}}&=\overline{h}_m\left\{\frac{(\widetilde{D}_{\tilde{B}})^{-1}}{(-\widetilde{C}_\infty+\widetilde{C}_w)}\right\}\widetilde{X},\\
\overline{C}_{\tilde{f}}&=\overline{\tau}_w\left\{\frac{(\widetilde{\rho})^{-1}}{(\widetilde{U}_w^{\,2})}\right\},\\
\overline{Nu}_{\tilde{X}}&=\overline{q}_w\left\{\frac{(\widetilde{k})^{-1}}{(-\widetilde{T}_\infty+\widetilde{T}_w)}\right\}\widetilde{X}.
\end{aligned} \tag{14}$$

In Eq. (14), the expressions of $\overline{h}_m$, $\overline{\tau}_w$, and $\overline{q}_w$ are taken as follows

$$\begin{aligned}
\overline{h}_m&=-(\widetilde{D}_{\tilde{B}})\left\{\frac{\partial\widetilde{C}}{\partial\widetilde{Y}}\right\}_{\tilde{Y}=0},\\
\overline{\tau}_w&=\left[\{\widetilde{\mu}+\widetilde{k}\}\left\{\frac{\partial\widetilde{U}}{\partial\widetilde{Y}}\right\}+\delta_1\left(2\left\{\frac{\partial\widetilde{U}}{\partial\widetilde{Y}}\right\}\left\{\frac{\partial\widetilde{U}}{\partial\widetilde{X}}\right\}+\left\{\frac{\partial^2\widetilde{U}}{\partial\widetilde{t}\partial\widetilde{Y}}\right\}+\left\{\frac{\partial^2\widetilde{U}}{\partial\widetilde{Y}^2}\right\}\widetilde{V}+\left\{\frac{\partial^2\widetilde{U}}{\partial\widetilde{X}\partial\widetilde{Y}}\right\}\widetilde{U}\right)+N^*\widetilde{k}\right]_{\tilde{Y}=0},\overline{q}_w\\
&=-(k_1)\left\{\frac{\partial\widetilde{T}}{\partial\widetilde{Y}}\right\}_{\tilde{Y}=0},
\end{aligned} \tag{15}$$

The execution of Eqs. (7) and (15) to Eq. (14), the following outcomes of quantities are acquired

3. Numerical algorithm

To solve the dimensionless Eqs. (8)-(12) through bvp4c technique in MATLAB, initially these equations with higher order takes the form of equations having first order derivatives. This conversion is accomplished by establishing the following new constraints:

$$\begin{aligned}
&\overline{Sh}_{\bar{x}}\left\{\frac{1}{(\overline{Re}_{\bar{x}})^{0.5}}\right\} = -\frac{d\Phi}{d\zeta}(0),\\
&\overline{C}_{\bar{f}}\left\{\frac{1}{(\overline{Re}_{\bar{x}})^{-0.5}}\right\} = \left\{\frac{d^2F}{d\zeta^2}(0)\right\} + (1-m_o)K\left\{\frac{d^2F}{d\zeta^2}(0)\right\} + \alpha^*\left[-\left\{\frac{d^3F}{d\zeta^3}(0)\right\}\{F(0)\}\right.\\
&\left.+3\left\{\frac{d^2F}{d\zeta^2}(0)\right\}\left\{\frac{dF}{d\zeta}(0)\right\} + S\left\{\frac{1}{2}\right\}\left(\left\{\frac{d^3F}{d\zeta^3}(0)\right\} + 3\left\{\frac{d^2F}{d\zeta^2}(0)\right\}\right)\right],\\
&\overline{Nu}_{\bar{x}}\left\{\frac{1}{(\overline{Re}_{\bar{x}})^{0.5}}\right\} = -\frac{d\theta}{d\zeta}(0),
\end{aligned} \tag{16}$$

$$\begin{aligned}
&F(\zeta) = X(1),\\
&\frac{dF}{d\zeta} = X(2),\\
&\frac{d^2F}{d\zeta^2} = X(3),\\
&\frac{d^3F}{d\zeta^3} = X(4),\\
&\frac{d^4F}{d\zeta^4} = XX1,
\end{aligned} \tag{17}$$

$$\begin{aligned}
XX1 = &-\frac{1}{\alpha^*\left\{\left\{\frac{1}{2}\right\}S\zeta - X(1)\right\}}\left(X(4)\{1+K\} + KX(5) - X(2)X(2)\right.\\
&+X(1)X(3) + Mexp(\zeta\lambda) + \alpha^*(2X(1)X(4) + S2X(4) - X(3)X(3))\\
&\left.-S\left\{X(2) + \zeta\left\{\frac{1}{2}\right\}X(3)\right\}\right),
\end{aligned} \tag{18}$$

$$\begin{aligned}
&G(\zeta) = X(5),\\
&\frac{dG}{d\zeta} = X(6),\\
&\frac{d^2G}{d\zeta^2} = XX2,
\end{aligned} \tag{19}$$

$$\begin{aligned}
XX2 = &-\frac{1}{\{1+K\{1/2\}\}}\left(X(6)X(1) - X(2)X(5) - K(2X(5) + X(3))\right.\\
&\left.-S\left(\left\{\frac{3}{2}\right\}X(5) + \left\{\frac{1}{2}\right\}X(6)\zeta\right)\right),
\end{aligned} \tag{20}$$

$$\begin{aligned}
&\theta(\zeta) = X(7),\\
&\frac{d\theta}{d\zeta} = X(8),\\
&\frac{d^2\theta}{d\zeta^2} = XX3,
\end{aligned} \tag{21}$$

$$\begin{aligned}
XX3 = &-\Pr\left((X(1)X(8) - X(2)X(7)) - S\left(X(7) + \left\{\frac{1}{2}\right\}X(8)\zeta\right)\right)\\
&-NbX(8)X(10)Pr - NtX(8)PrX(8) - PrX(2)M^*X(2)Ec\\
&-DuXX4Pr,
\end{aligned} \tag{22}$$

$$\begin{aligned}
&\Phi(\zeta) = X(9)\\
&\frac{d\Phi}{d\zeta} = X(10)\\
&\frac{d^2\Phi}{d\zeta^2} = XX4
\end{aligned} \tag{23}$$

$$\begin{aligned}
XX4 = &-\left\{\frac{N_t}{N_b}\right\}XX3 - Sc\left(X(1) - \zeta\left\{\frac{1}{2}\right\}S\right)X(10) - ScXX3Sr\\
&+\kappa_o e^{\left(\frac{E}{1+X(7)\theta_w}\right)}Sc(1+X(7)\theta_w)^{\tilde{n}}),
\end{aligned} \tag{24}$$

Relevant conditions are defined as follows

$$\begin{aligned}
&X0(5) + m_oX0(3),\\
&X0(9) - 1;\\
&X0(1);\\
&X0(8) + \gamma^*\{1 - X0(7)\};\\
&X0(2) - 1;\\
&Xinf(7);\\
&Xinf(2);\\
&Xinf(5);\\
&Xinf(9);\\
&Xinf(3).
\end{aligned} \tag{25}$$

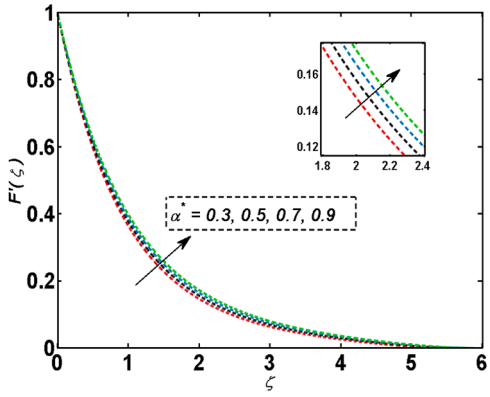

Fig. 2. $F'(\zeta)$ curve via α* parameter.

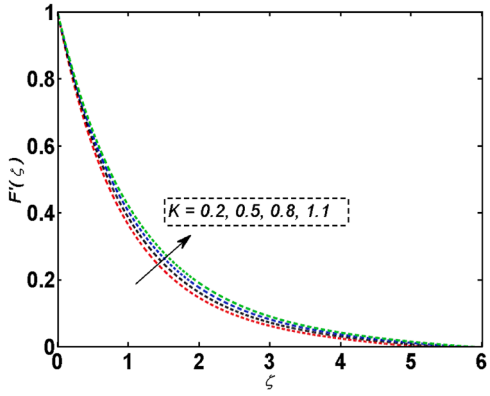

Fig. 3. $F(\zeta)$ curve via K parameter.

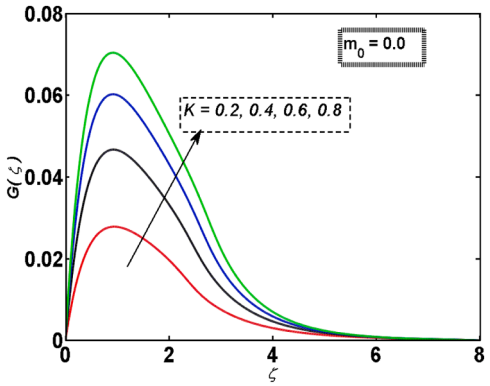

Fig. 4. $G(\zeta)$ curve via K parameter regarding $m_o = 0.0$.

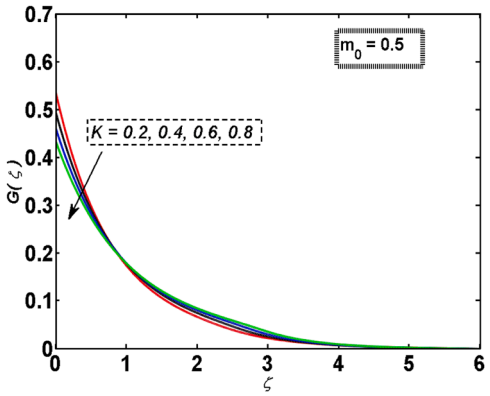

Fig. 5. $G(\zeta)$ curve via K parameter regarding $m_o = 0.5$.

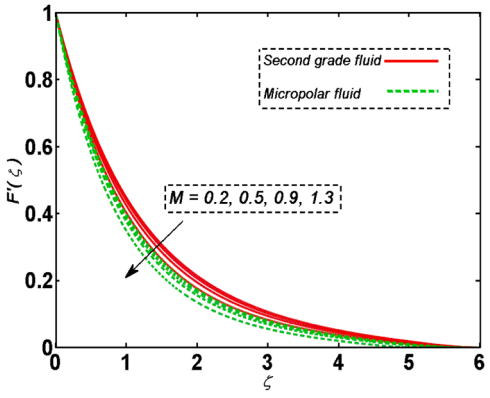

Fig. 6. $F'(\zeta)$ curve via M parameter.

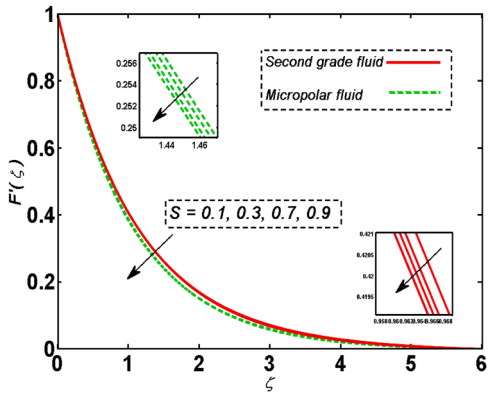

Fig. 7. $F'(\zeta)$ curve via S parameter.

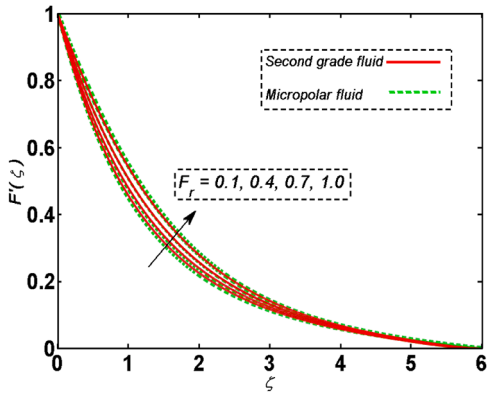

Fig. 8. $F'(\zeta)$ curve via F_r parameter.

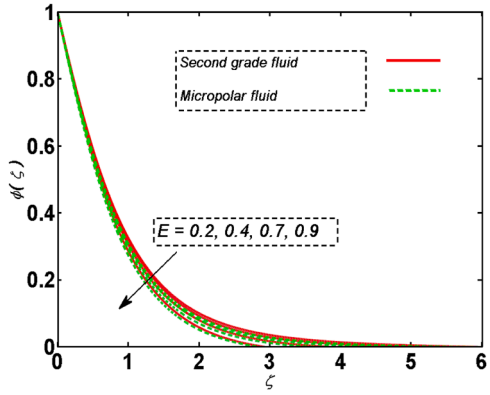

Fig. 9. $\Phi(\zeta)$ curve via E parameter.

4. Graphs and discussion

This section has the objective of scrutinizing the performance of temperature, microrotation velocity, concentration, and translational velocity relative to both micropolar fluid and second grade fluid with pertinent distinct parameters. The different physical attributes of both concerned fluids are graphically explored and compared in the context of pertinent parameters. By taking into account both weak and strong concentrations of microelements, micro rotational velocity is demonstrated. Fig. 2 manifests the consequence of the second-grade fluid parameter on the distribution of translational velocity. This graphic yield the result that an augmentation of the fluid parameter upsurges the translational velocity. The increment of the considered velocity is acquired due to the inverse connection between viscosity attribute of fluid and concerned fluid parameter. There is a declination in the fluid viscosity with the increment of the fluid parameter. It is a natural fact that a fluid having minimizing viscosity has lower opposition in its movement. Due to this reason, the translational fluid velocity depicts an ascending nature. On the other hand, the curve of translational velocity regarding high intensity of the micropolar fluid parameter is portrayed in Fig. 3. This graphical result in Fig. 3 is same as in the case of Fig. 2. The fact behind this intensification of translational velocity is again the development of reverse link within relevant fluid parameter and viscosity. By taking into account both strong and weak concentrated microelements, the rotational velocity of microparticles is elucidated in Figs. 4 and 5 corresponding to fluid parameter. In the context of strong concentration $m_o = 0.0$, the fluid parameter lifts up the micro rotational

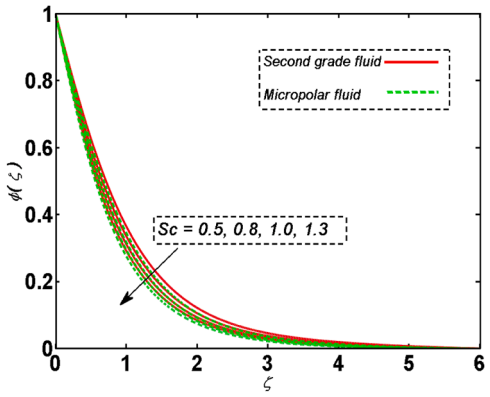

Fig. 10. $\Phi(\zeta)$ curve via *Sc* parameter.

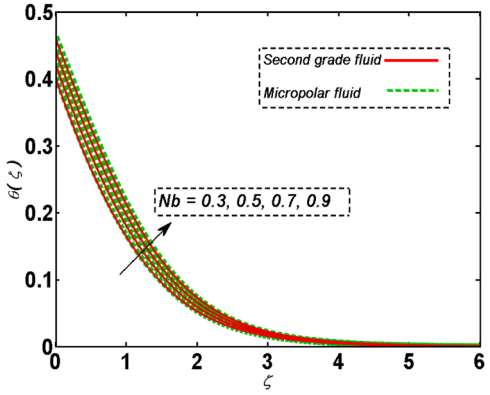

Fig. 11. θ(ζ) curve via *Nb* parameter.

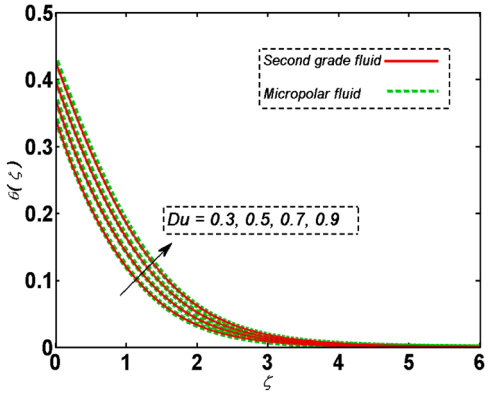

Fig. 12. θ(ζ) curve via *Du* parameter.

velocity in Fig. 4. With the strong concentration, more micro particles rotate within the concerned fluid and consequently augment the concerned velocity. On the other hand, in Fig. 5, the weak concentration implies that near the surface, the rotatory movement of microelements becomes negligible. As a result, the rotational motion depicts a reduction nature across the surface. The purpose of sketching Fig. 6 is to compare the effectiveness of velocity profiles of both considered fluid regarding higher magnitude of the magnetic parameter. It is interesting to observe that the magnetic parameter has the same influence on both fluids' movement. In the context of both considered fluid, the magnetic field with higher amplitude lowers the motion due to the involvement of Lorentz resistive force. Along the opposite movement direction of the fluids, this strongest force participates in developing difficulties in their motion. Consequently, both considered fluids have the diminishing

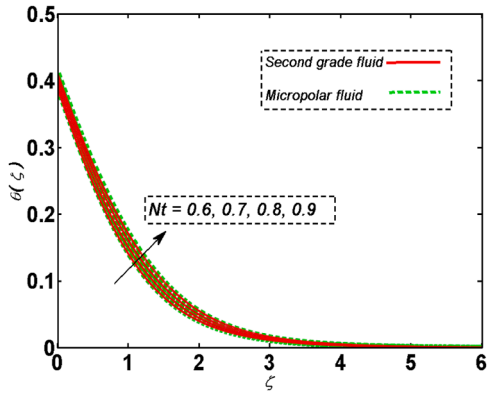

Fig. 13. θ(ζ) curve via *Nt* parameter.

Table 1
Numerical exploration of physical quantities regarding pertinent parameters.

N_b	N_t	Sc	$\overline{Sh}_{\bar{x}}\left\{\frac{1}{(\overline{Re}_{\bar{x}})^{0.5}}\right\}$	$\overline{Nu}_{\bar{x}}\left\{\frac{1}{(\overline{Re}_{\bar{x}})^{0.5}}\right\}$
0.2	–	–	0.2121127	0.4242254
0.4	–	–	0.4060563	0.5378120
0.6	–	–	0.7070423	0.7651234
–	0.3	–	0.2119549	0.4239097
–	0.5	–	0.5570667	0.5684819
–	0.7	–	0.6514468	0.6483829
–	–	0.5	0.6700689	0.5743448
–	–	0.6	0.6699165	0.5742141
–	–	0.7	0.6697682	0.5740871

Table 2
Numerical exploration of physical quantity $\overline{C}_{\bar{f}}\left\{\frac{1}{(\overline{Re}_{\bar{x}})^{-0.5}}\right\}$ regarding pertinent parameters.

K	α^*	S	$\overline{C}_{\bar{f}}\left\{\frac{1}{(\overline{Re}_{\bar{x}})^{-0.5}}\right\}$
0.2	0.1	2.0	0.5095381
0.4	–	–	0.4869802
0.6	–	–	0.4711083
–	0.3	–	0.2499768
–	0.5	–	0.3340771
–	0.7	–	0.4978418
–	–	1.9	0.3694771
–	–	1.8	0.2574789
–	–	1.7	0.0749288

nature in the context of the magnetic parameter. To observe the consequence of unsteadiness parameter regarding the fields of both concerned fluid, Fig. 7 is sketched. As the unsteadiness parameter enhance in its magnitude, there exists a deterioration in the context of both fluids' velocity curves. The initial stretching rate face a reduction with the improved unsteadiness parameter. As a result, the considered surface has lower scratchable velocity. With this reduction, the considered fluid's curves demonstrate reducing nature. Fig. 8 manifests the influence of Darcy Forchheimer parameter on velocity field in the context of both fluids. this graphic portrays the augmented nature of the considered field. However, this impact is more effective in the case of micropolar fluid. Fig. 9 signifies the concentration of both considered fluids regarding improved activation energy parameter. Physically, the diffusion of a solute in both fluids strongly depend on the energy obstacles which takes existence with the improved activation energy. The activation energy parameter with its higher amplitude yields strongest obstacles in the diffusion process of solute in both fluids. Consequently, both considered fluids portray the deteriorating nature. Fig. 10 is

organized to discover the consequence of the Schmidt number on both fluids regarding their concentration fields. Schmidt number has connection with the diffusion procedure in concerned fluids. The diffusion procedure undergoes a reduction level corresponding to the improved Schmidt number. Fig. 11 portray the significance of Brownian motion parameter for both fluids regarding their temperature fields. The increment of Brownian motion parameter upsurges the randomly movement of molecules within both fluids which consequently lifts up the distributions of concentration. The enhanced nature of temperature fields concerning both fluids in the context of the Dufour number is deliberated in Fig. 12. With the improvement of the Dufour number, there exists an augmentation in heat transfer mechanisms of both fluids. The purpose of creating Fig. 13 is to explore the influence of the thermophoresis parameter in the context of both fluids regarding their concentrations. With the improved concerned parameter, more particles start to move from higher concentrated place to lower concentrated and consequently both fluids exhibit upgraded concentration profiles.

To perceive the numerical algorithm of physical quantities related to the current study for both considered fluids, Tables 1 and 2 are prepared. Both quantities of Sherwood number and Nusselt number are analyzed in Table 1 in the context of emerging parameters. It is significant from this calculation that both concerned quantities depict a reduction process by lifting up the Schmidt number. On the other hand, the same quantities regarding Brownian motion and thermophoresis parameters yields augmented behavior. The other quantity of skin friction coefficient is deliberated in Table 1 in the context of pertinent parameters. The concerned quantity in the context of micropolar fluid parameter exhibit declining procedure. On the other hand, in the case of second grade fluid parameter, this quantity depicts the opposite phenomenon. The influence of unsteadiness parameter on both considered fluids is to lower the surface drag force.

5. Conclusion

This section concludes the main result developed form the comparative flow performance of two distinct second grade fluid and micropolar fluid. The present study covers different aspects related to the thermal and flow characteristics in the context of numerous impacts. Both concerned fluids are briefly discussed with graphical comparative outcomes. These findings are valuable in the domains of science and engineering. Key observations are outlined as follows

- In the context of both considered fluids, temperature curve goes up to the supreme level with the relationship of thermophoresis.
- The field of concentration regarding both fluids is an abating function of activation energy parameter.
- The more concentrated microelements upsurge the rotational motion and weak concentrated elements lowers the rotatory movement of micro molecules.
- For both fluids, the unsteadiness and magnetic parameters curtail the velocity distributions.
- Schmidt number with greater intensification develops a curtailment in concentration fields.
- Temperature fields regarding both fluids depict a higher level with the significant Brownian motion parameter.

Declaration of competing interest

The authors declared that they have no conflict of interest and the paper presents their own work which does not been infringe any third-party rights, especially authorship of any part of the article is an original contribution, not published before and not being under consideration for publication elsewhere

Data availability

Data will be made available on request.

References

1. Eringen AC. Theory of micropolar fluids. *J. Math. Mech.* 1966;1:1–8.
2. Erigen AC. Theory of thermomicropolar fluids. *J. Math. Anal. Appl.* 1972;38(2):480–496.
3. Chamkha AJ, Mohamed RA, Ahmed SE. Unsteady MHD natural convection from a heated vertical porous plate in a micropolar fluid with Joule heating, chemical reaction and radiation effects. *Meccanica.* 2011;46:399–411.
4. Sheikholeslami M, Hatami M, Ganji DD. Micropolar fluid flow and heat transfer in a permeable channel using analytical method. *J. Mol. Liq.* 2014;194:30–36.
5. Pal D, Chatterjee S. Effects of radiation on Darcy-Forchheimer convective flow over a stretching sheet in a micropolar fluid with non-uniform heat source/sink. *J. Appl. Fluid Mech.* 2014;8(2):207–212.
6. Zaimi K, Ishak A. Stagnation-Point Flow and Heat Transfer over a Nonlinearly Stretching/Shrinking Sheet in a Micropolar Fluid. *In Abstract and Applied Analysis.* 2014;2014(1), 261630.
7. Abdollahzadeh Jamalabadi MY. Entropy generation in boundary layer flow of a micro polar fluid over a stretching sheet embedded in a highly absorbing medium. *Front. Heat Mass Transf.* 2015;6(1). https://doi.org/10.5098/hmt.6.7.
8. Noreen S, Fatima K, Tripathi D. Electroosmosis-driven heat transfer in Jeffrey fluid flow through tapered porous channel. *Numer. Heat Transf.; A: Appl.* 2024;85(15):2473–2497.
9. Fatunmbi EO, Adeniyan A. Heat and mass transfer in MHD micropolar fluid flow over a stretching sheet with velocity and thermal slip conditions. *Open J. Fluid Dyn.* 2018;8:195–215.
10. Mandal IC, Mukhopadhyay S. Nonlinear convection in micropolar fluid flow past an exponentially stretching sheet in an exponentially moving stream with thermal radiation. *Mech. Adv. Mater. Struct.* 2019;26(24):2040–2046.
11. Dawar A, Shah Z, Tassaddiq A, Islam S, Kumam P. Joule heating in magnetohydrodynamic micropolar boundary layer flow past a stretching sheet with chemical reaction and microstructural slip. *Case Stud. Therm. Eng.* 2021;25, 100870.
12. Ishtiaq B, Zidan AM, Nadeem S, Alaoui MK. Analysis of entropy generation in the nonlinear thermal radiative micropolar nanofluid flow towards a stagnation point with catalytic effects. *Phys. Scr.* 2022;97(8), 085204.
13. Yasir M, Khan M, Al-Zubaidi A, Saleem S. Arrhenius activation energy effect in thermally viscous dissipative flow of micropolar material with gyrotactic microorganisms. *Alex. Eng. J.* 2023;84:204–214.
14. Yasir M, Bilal S, Ahammad NA, Elseesy IE. Thermal irregular generation and absorption of nanoscale energy transportation of thermodynamic material of a micropolar fluid. *Ain Shams Eng. J.* 2024;15(9), 102948.
15. Jamil M, Rauf A, Fetecau C, Khan NA. Helical flows of second grade fluid due to constantly accelerated shear stresses. *Commun. Nonlinear Sci. Numer. Simul.* 2011;16(4):1959–1969.
16. Turkyilmazoglu M. Dual and triple solutions for MHD slip flow of non-Newtonian fluid over a shrinking surface. *Comput. Fluids.* 2011;70:53–58.
17. Zheng L, Niu J, Zhang X, Gao Y. MHD flow and heat transfer over a porous shrinking surface with velocity slip and temperature jump. *Math. Comp. Model.* 2012;56:133–144.
18. Srinivasa RK, Reddy BR, Rao PK. Thermal effects in Stokes' second problem for unsteady second grade fluid flow through a porous medium under effect of a magnetic field. *J. Math.* 2013;7(2):5–14.
19. Bhadauria BS, Kiran P. Weak nonlinear oscillatory convection in a viscoelastic fluid-saturated porous medium under gravity modulation. *Transp. Porous Media.* 2014;104(3):451–467.
20. Rahman M, Khan M, Manzur M. Homogeneous-heterogeneous reactions in modified second grade fluid over a non-linear stretching sheet with Newtonian heating. *Results Phys.* 2017;7:4364–4370.
21. Shojaei A, Amiri AJ, Ardahaie SS, Hosseinzadeh K, Ganji DD. Hydrothermal analysis of Non-Newtonian second grade fluid flow on radiative stretching cylinder with Soret and Dufour effects. *Case Stud. Therm. Eng.* 2019;13, 100384.
22. Vaidya H, Prasad KV, Gudekote M, Tripathi D, Choudhari R. A comprehensive analysis of magnetized non-newtonian nanofluids' peristaltic mechanism for optimized fluid flow and heat transfer. *Case Stud. Therm. Eng.* 2024;61, 104929.
23. Bhandari DS, Tripathi D, Prakash J. Insight into Newtonian fluid flow and heat transfer in vertical microchannel subject to rhythmic membrane contraction due to pressure gradient and buoyancy forces. *Int. J. Heat Mass Transf.* 2022;184, 122249.
24. Nadeem S, Ishtiaq B, Almutairi S, Ghazwani HA. Impact of Cattaneo–Christov double diffusion on 3d stagnation point axisymmetric flow of second-grade nanofluid towards a riga plate. *Int. J. Mod. Phys. B.* 2022;36(29), 2250205.
25. Abbas N, Tumreen M, Shatanawi W, Qasim M, Shatnawi TA. Thermodynamic properties of second grade nanofluid flow with radiation and chemical reaction over slendering stretching sheet. *Alex. Eng. J.* 2023;70:219–230.
26. Nadeem S, Tumreen M, Ishtiaq B, Abbas N, Shatanawi W. Second-grade nanofluid flow above a vertical slandering Riga surface with double diffusion model. *Int. J. Mod. Phys. B.* 2022;36(32), 2250237.
27. Cham A, Mustafa M. Exploring the dynamics of second-grade fluid motion and heat over a deforming cylinder or plate affected by partial slip conditions. *Arab. J. Sci. Eng.* 2024;49(2):1505–1514.

28. Padhi S, Nayak I. Unsteady EMHD free convective second grade fluid flow past an exponentially accelerated vertical porous plate. *Numer. Heat Transf. B*. 2023;83(3):102–119.
29. Choi SU, Eastman JA. *Enhancing Thermal Conductivity of Fluids with Nanoparticles*. Argonne, IL (United States): Argonne National Lab. (ANL); 1995.
30. Noghrehabadi A, Saffarian MR, Pourrajab R, Ghalambaz M. Entropy analysis for nanofluid flow over a stretching sheet in the presence of heat generation/absorption and partial slip. *J. Mech. Sci. Technol.* 2013;27:927–937.
31. Kandelousi MS. KKL correlation for simulation of nanofluid flow and heat transfer in a permeable channel. *Phys. Lett. A*. 2014;378(45):3331–3339.
32. Turkyilmazoglu M. Analytical solutions of single and multi-phase models for the condensation of nanofluid film flow and heat transfer. *Eur. J. Mech. B*. 2015;53:272–277.
33. Bhatti MM, Shahid A, Abbas T, Alamri SZ, Ellahi R. Study of activation energy on the movement of gyrotactic microorganism in a magnetized nanofluids past a porous plate. *Processes*. 2020;8(3):328.
34. Nasir S, Berrouk AS, Tassaddiq A, Aamir A, Akkurt N, Gul T. Impact of entropy analysis and radiation on transportation of MHD advance nanofluid in porous surface using Darcy-Forchheimer model. *Chem. Phys. Lett.* 2023;811, 140221.
35. Tripathi D, Bhandari DS, Anwar Bég O. Thermal effects on SARS-CoV-2 transmission in peristaltic blood flow: mathematical modeling. *Phys. Fluids*. 2022;34(6), 061904.
36. Yasir M, Ahmed A, Khan M, Usman M. Theoretical investigation of time-dependent Oldroyd-B nanofluid flow containing gyrotactic microorganisms due to stretching cylinder. *Waves Random Complex Media*. 2022:1–9. https://doi.org/10.1080/17455030.2022.2040758.
37. Akram J, Akbar NS, Tripathi D. Thermal analysis on MHD flow of ethylene glycol-based BNNTs nanofluids via peristaltically induced electroosmotic pumping in a curved microchannel. *Arab. J. Sci. Eng.* 2022;47(6):7487–7503.
38. Nasir S, Berrouk AS, Aamir A, Shah Z. Entropy optimization and heat flux analysis of Maxwell nanofluid configurated by an exponentially stretching surface with velocity slip. *Sci. Rep.* 2023;13(1):2006.
39. Ahmad L, Latif M, Eldin SM. Chemically reactive and thin film flow analysis of cross nano-liquid over a moving surface. *Arab. J. Chem.* 2023;16(11), 105264.
40. Nasir S, Berrouk AS, Aamir A, Gul T. Significance of chemical reactions and entropy on Darcy-forchheimer flow of H2O and C2H6O2 convening magnetized nanoparticles. *Int. J. Thermofluids*. 2023;17, 100265.
41. Al Qahtani SA, Ahmad L, Khan IU, Pathak P. Local non-similar solution of radiative and magnetized flow of non-Newtonian liquid over a gravitationally affected porous surface with Newtonian heating effect. *J. Eng. Res.* 2023;11(3):18–27.
42. Bhardwaj A, Kumar A, Tripathi D. Multi-membranes-based pumping flow of nanofluids: application in thermofluidic system. *Numer. Heat Transf. A*. 2024:1–27. https://doi.org/10.1080/10407782.2024.2355367.
43. Ishtiaq B, Nadeem S, Abbas N. Theoretical study of two-dimensional unsteady Maxwell fluid flow over a vertical Riga plate under radiation effects. *Sci. Iran.* 2022;29(6):3072–3083.
44. Madan Kumar R, Srinivasa Raju R, Kumar MA, Venkateswarlu B. A numerical study of thermal and diffusion effects on MHD Jeffrey fluid flow over a porous stretching sheet with activation energy. *Numer. Heat Transf. A*. 2024:1–22. https://doi.org/10.1080/10407782.2024.2319344.